Electronic Supplementary Information

All reagents were used as received from commercial suppliers. High-grade solvents were obtained from a MBRAUN MB-SPS 800 solvent purification system. Starting materials, $(N(n\mathrm{Bu})_4)[M^{III}L(acac)_2]$[1] and $(N(n\mathrm{Bu})_4)_2[Mo_5O_{13}(OMe)_4(NO)(Na(MeOH))]$,[2] were synthesised as previously published.

1 – Instrumentation

NMR experiments were recorded on a Bruker BioSpin 400 MHz NMR spectrometer. Electrospray mass spectra (ESI-MS) were performed using a MAT 95-maXis II mass spectrometer. UV-Vis electron absorption spectroscopy experiments were measured on a Shimadzu UV-2600 spectrophotometer using 10 mm quartz glass cuvettes. IR spectra were collected on a Bruker VERTEX 70 FT-IR spectrometer coupled with a RAM II FT-Raman module. Magnetic properties were determined using a Quantum Design MPMS-5XL SQUID magnetometer for direct current (dc) and alternating current (ac) measurements. Microcrystalline samples of **2** and **3** was compacted and immobilised into cylindrical PTFE sample holders. Experimental dc data were recorded at 0.1 T and 1.0 T in the temperature range 2.0–290 K and at 2.0 K in the field range 0.1–5.0 T. Experimental ac data were collected at various static bias fields between 0 and 1000 Oe in the temperature range 2.0–50 K and frequency range 3–1000 Hz using an amplitude of B_{ac} = 3 G. No relevant out-of-phase signals were detected for **2** in this parameter range. All data were corrected for the diamagnetic contributions of the sample holders and the complex using the data of **1** as diamagnetic reference ($\chi_{m,dia}$ / 10^{-4} cm^3 mol^{-1} = –9.21 (**2**), –9.22 (**3**)). Single-crystal X-ray diffraction data for **1**−**3** were collected on STOE STADIVARI (**1**) and on a Rigaku SuperNova (**2** and **3**) diffractometers with MoKα radiation (λ = 0.71073 Å) at 100 K. Powder X-ray diffraction was recorded at room temperature on a STOE StadiP diffractometer.

2 – Synthesis and analytical characterisation

$(N(n\mathrm{Bu})_4)_2[M^{III}L\{Mo_5O_{13}(OMe)_4(NO)\}]$

$(N(n\mathrm{Bu})_4)[M^{III}L(acac)_2]$ (0.1 mmol) and $(N(n\mathrm{Bu})_4)_2[Mo_5O_{13}(OMe)_4(NO)(Na(MeOH))]$ (113.52 mg, 0.1 mmol) were dissolved in 50 mL of dry acetonitrile and refluxed at 90 °C for 12 hours. The resulting solution was then cooled down, filtered and evaporated to a brown oil. Consecutive re-dissolution, filtration and evaporation of this crude product in dichloromethane, acetonitrile and tetrahydrofuran yielded a brown solid free of unreacted starting materials. This solid was washed with 500 mL diethyl ether and evaporated to afford a brown solid. Brown rod-shaped single crystals were obtained by slow evaporation of dichloromethane/*n*-hexane (1/3, v/v) mix solution after one week. Yield: 32 mg (15%) for Y; 45 mg (21%) for Gd; 50 mg (23%) for Dy.

$(N(nBu)_4)_2[Y^{III}L\{Mo_5O_{13}(OMe)_4(NO)\}]$ (1)

^{1}H NMR (400MHz, CD_3CN): δ 6.98 (s, 4H, Ar*H*), 6.93 (s, 4H, Ar*H*), 4.64 (s, 12H, $\{Mo_5O_{13}(OMe)_4(NO)\}$-OC*H*$_3$), 4.34 (d, *J* = 11.5 Hz, 4H, C*H*$_{2axial}$), 3.76 (s, 6H, OC*H*$_3$), 3.10–3.05 (m, 8H, N(*n*Bu)$_4$–NC*H*$_2$), 3.03 (d, *J* = 11.5 Hz, 4H, C*H*$_{2equatorial}$), 1.63–1.55 (m, 8H, N(*n*Bu)$_4$–NCH$_2$C*H*$_2$), 1.40–1.31 (m, 8H, N(*n*Bu)$_4$–N(CH$_2$)$_2$C*H*$_2$), 1.22 (s, 18H, ^{t}Bu–C*H*$_3$), 1.07 (s, 18H, ^{t}Bu–C*H*$_3$), 0.97 (t, *J* = 7.3 Hz, 12H, N(*n*Bu)$_4$–N(CH$_2$)$_3$C*H*$_3$) ppm.

ESI-HRMS *m/z*: found 802.9335 $[M - 2\ N(nBu)_4]^{2-}$ (34.3%), calculated for $[C_{50}H_{70}NO_{22}Mo_5Y]^{2-}$ 802.9385; *m/z*: found 1848.1571 $[M - N(nBu)_4]^{1-}$ (7.6%), calculated for $[C_{66}H_{106}N_2O_{22}Mo_5Y]^{1-}$ 1848.1614. M here stands for $(N(nBu)_4)_2[Y^{III}L\{Mo_5O_{13}(OMe)_4(NO)\}]$.

Elemental analysis calculated for $C_{82}H_{142}N_3O_{22}Mo_5Y$ $(N(nBu)_4)_2[Y^{III}L\{Mo_5O_{13}(OMe)_4(NO)\}]$: C, 47.11; H, 6.85; N, 2.01 %. Found C, 47.18; H, 6.89; N, 2.02 %.

IR (ν / cm^{-1}): ~2958–2873 (m, C–H str.), ~1622 (m, N–O str.), ~1479–1431 (m, arC–C$_{str.}$/CH$_{2bend.}$/CH$_{3\ bend.}$), ~1334 (m, CH$_3$ bend.), ~1213 (w, C–O str.), ~1037 (m, C–O$_{POM}$ str.), ~928–864 (s, (Mo–O$_t$)$_{POM}$ str.) and ~ 681 (vs, (Mo–O–Mo)$_{POM}$ str.).

UV-Vis {CH_3CN, λ / nm (ε / M^{-1} cm^{-1})}: 244 (1.23×10^4), 306 (5.98×10^3).

Crystallographic data for **1** (CCDC 2143146): $C_{84.5}H_{147}N_3O_{22}Cl_5Mo_5Y$, M_r = 2302.90 g mol^{-1}, brown rod, 0.22 x 0.11 x 0.05 mm^3, triclinic, space group *P*−1, *a* = 13.449(3) Å, *b* = 14.984(3), *c* = 27.024(5) Å, *α* = 100.93(3)°, *β* = 102.94(3), *γ* = 101.77(3)°, *V* = 5036(2) Å^3, *Z* = 2, STOE STADIVARI diffractometer, MoKα radiation (*λ* = 0.71073 Å), *T* = 100 K, 92044 reflections collected, 17716 unique (R_{int} = 0.0927), 11169 observed ($I > 2\sigma(I)$). Final *GooF* = 1.043, *R1* = 0.0794 ($I > 2\sigma(I)$) and *wR2* = 0.2388 (all data).

$(N(nBu)_4)_2[Gd^{III}L\{Mo_5O_{13}(OMe)_4(NO)\}]$ (2)

ESI-HRMS *m/z*: found 836.9437 $[M - 2\ N(nBu)_4]^{2-}$ (32.9%), calculated for $[C_{50}H_{70}NO_{22}Mo_5Gd]^{2-}$ 836.9474; *m/z*: found 1916.1709 $[M - N(nBu)_4]^{1-}$ (100%), calculated for $[C_{66}H_{106}N_2O_{22}Mo_5Gd]^{1-}$ 1916.1796. M here stands for $(N(nBu)_4)_2[Gd^{III}L\{Mo_5O_{13}(OMe)_4(NO)\}]$.

Elemental analysis calculated for $C_{82}H_{142}N_3O_{22}Mo_5Gd$ $(N(nBu)_4)_2[Gd^{III}L\{Mo_5O_{13}(OMe)_4(NO)\}]$: C, 45.61; H, 6.63; N, 1.95 %. Found C, 45.84; H, 6.86; N, 1.98 %.

IR (ν / cm^{-1}): ~2958–2873 (m, C–H str.), ~1622 (m, N–O str.), ~1479–1431 (m, arC–C$_{str.}$/CH$_{2bend.}$/CH$_{3\ bend.}$), ~1334 (m, CH$_3$ bend.), ~1213 (w, C–O str.), ~1037 (m, C–O$_{POM}$ str.), ~928–864 (s, (Mo–O$_t$)$_{POM}$ str.) and ~ 681 (vs, (Mo–O–Mo)$_{POM}$ str.).

UV-Vis {CH_3CN, λ / nm (ε / M^{-1} cm^{-1})}: 244 (1.51×10^4), 306 (4.63×10^3).

Crystallographic data for **2** (CCDC 2143147): $C_{83}H_{144}N_3O_{22}Cl_2GdMo_5$, M_r = 2243.85 g mol^{-1}, brown rod, 0.20 x 0.055 x 0.03 mm^3, monoclinic, space group *C*2/*c*, *a* = 67.2987(15) Å, *b* = 12.5266(2), *c* = 23.4455(4) Å, *β* = 103.345(2), *V* = 19231.4(6) Å^3, *Z* = 8, Rigaku SuperNova diffractometer, MoKα radiation (*λ* = 0.71073 Å), *T* = 100 K, 84378 reflections collected, 16931 unique (R_{int} = 0.0770), 12688 observed ($I > 2\sigma(I)$). Final *GooF* = 1.052, *R1* = 0.0430 ($I > 2\sigma(I)$) and *wR2* = 0.1039 (all data).

$(N(nBu)_4)_2[Dy^{III}L\{Mo_5O_{13}(OMe)_4(NO)\}]$ (3)

ESI-HRMS *m/z*: found 839.9466 $[M - 2\ N(nBu)_4]^{2-}$ (12.1%), calculated for $[C_{50}H_{70}NO_{22}Mo_5Dy]^{2-}$ 839.9495; *m/z*: found 1922.1775 $[M - N(nBu)_4]^{1-}$ (100%), calculated for $[C_{66}H_{106}N_2O_{22}Mo_5Dy]^{1-}$ 1922.1836. M stands for $(N(nBu)_4)_2[Dy^{III}L\{Mo_5O_{13}(OMe)_4(NO)\}]$.

Elemental analysis calculated for $C_{82}H_{142}N_3O_{22}Mo_5Dy$ $(N(nBu)_4)_2[Dy^{III}L\{Mo_5O_{13}(OMe)_4(NO)\}]$: C, 45.51; H, 6.61; N, 1.94 %. Found C, 45.70; H, 6.56; N, 2.00 %.

IR (ν / cm^{-1}): ~2958–2873 (m, C–H str.), ~1622 (m, N–O str.), ~1479–1431 (m, arC–$C_{str.}$/$CH_{2bend.}$/$CH_{3\ bend.}$), ~1334 (m, CH_3 bend.), ~1213 (w, C–O str.), ~1037 (m, C–O_{POM} str.), ~928–864 (s, $(Mo–O_t)_{POM}$ str.) and ~ 681 (vs, $(Mo–O–Mo)_{POM}$ str.).

UV-Vis {CH_3CN, λ / nm (ε / M^{-1} cm^{-1})}: 244 (1.62×10^4), 306 (5.98×10^3).

Crystallographic data for **3** (CCDC:2143149): $C_{83}H_{144}N_3O_{22}Cl_2Mo_5Dy$, *M*r = 2249.10 g mol^{-1}, brown rod, 0.416 x 0.107 x 0.074 mm^3, monoclinic, space group *C*2/*c*, *a* = 67.0340(6) Å, *b* = 12.5392(1), *c* = 23.4462(2) Å, β = 103.174(1), *V* = 19189.1(3) $Å^3$, *Z* = 8, Rigaku SuperNova diffractometer, MoKα radiation (λ = 0.71073 Å), *T* = 100 K, 172457 reflections collected, 16905 unique (R_{int} = 0.0764), 14508 observed ($I > 2\sigma(I)$). Final *GooF* = 1.084, *R1* = 0.0388 ($I > 2\sigma(I)$) and *wR2* = 0.0902 (all data).

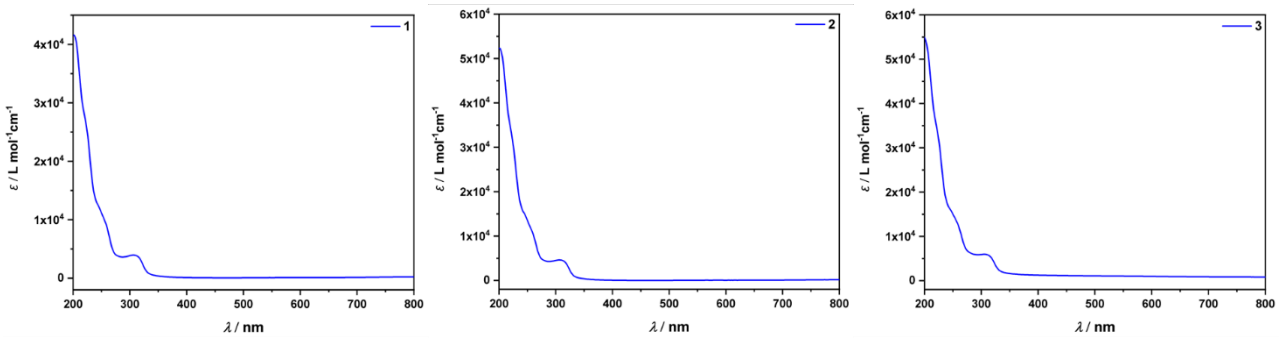

Fig. S1. UV-Vis spectra of CH_3CN solutions of complexes **1**–**3** (left to right). The curves present one peak at 306 nm, attributed to a π–π* transition centred on the phenyl rings of the TBC[4] ligand, and one shoulder peak at 244 nm, attributed to a n–π* transition of nitroso group from the $[Mo_5O_{13}(OMe)_4(NO)]^{3-}$ unit.

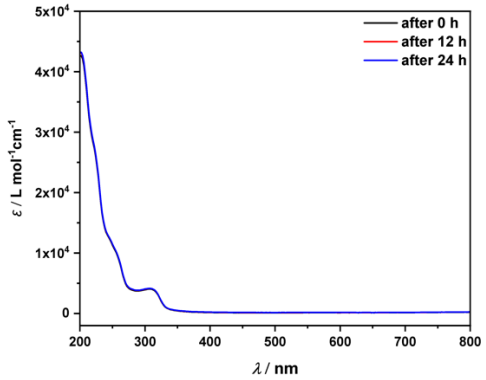

Fig. S2. UV-Vis spectra of a CH_3CN solution of complex **1** after 0 h (black line), 12 h (red line) and 24 h (blue line). The curves remain almost unchanged, indicating complex **1** remains stable in CH_3CN solution.

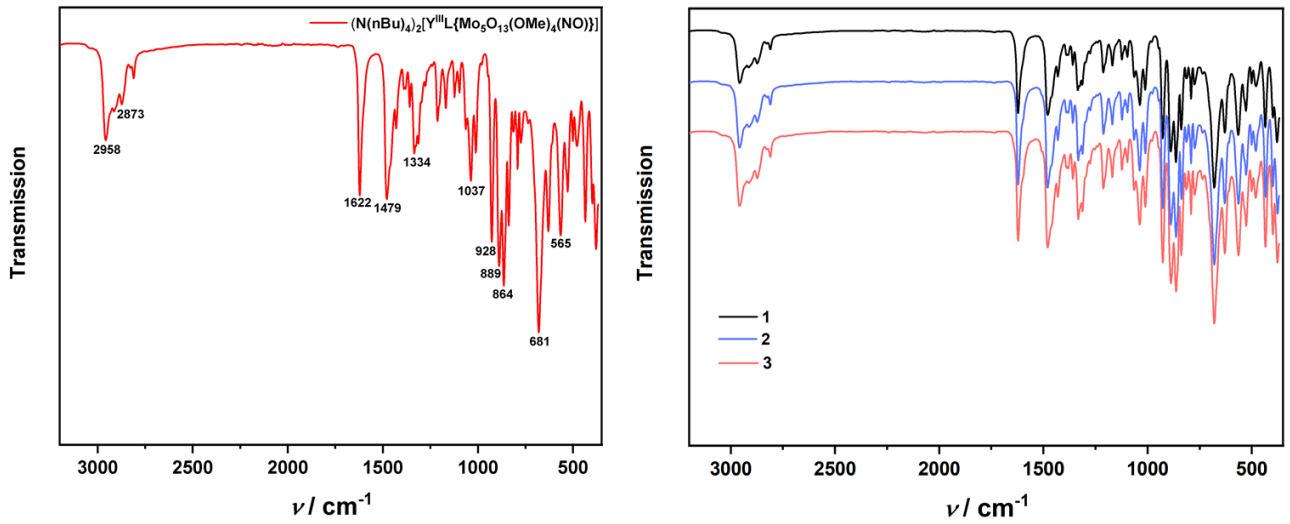

Fig. S3. IR spectra of $(N(nBu)_4)_2[Y^{III}L\{Mo_5O_{13}(OMe)_4(NO)\}]$ (**1**) (**Left**), and complexes **1**–**3** (**Right**). FT–IR spectra (**1**) display vibrations associated with ν(C–H) ~2958–2873 cm^{-1} (m), $\nu(N–O)_{[Mo5O13(OMe)4(NO)]}$ ~1622 cm^{-1} (m), overlapping vibrations of ν(arC–C)/$\delta(CH_2)$/$\delta_{as}(CH_3)$ ~1479–1431 cm^{-1} (m), $\delta_s(CH_3)$ ~1334 cm^{-1} (m), ν(C–O) ~1213 cm^{-1} (w), $\nu(C–O)_{[Mo5O13(OMe)4(NO)]}$ ~1037 cm^{-1} (m), $\nu(Mo–O_t)_{[Mo5O13(OMe)4(NO)]}$ ~ 928–864 cm^{-1} (s) and $\nu(Mo–O–Mo)_{[Mo5O13(OMe)4(NO)]}$ ~ 681 cm^{-1} (vs).

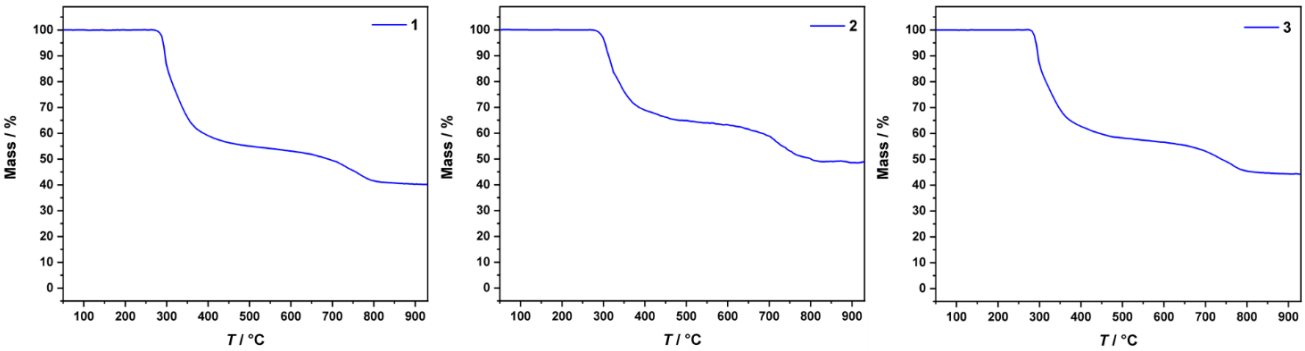

Fig. S4. Thermogravimetric analysis (TGA) for complexes **1**–**3** (left to right). Complexes exhibit thermal stability up to ~280 °C.

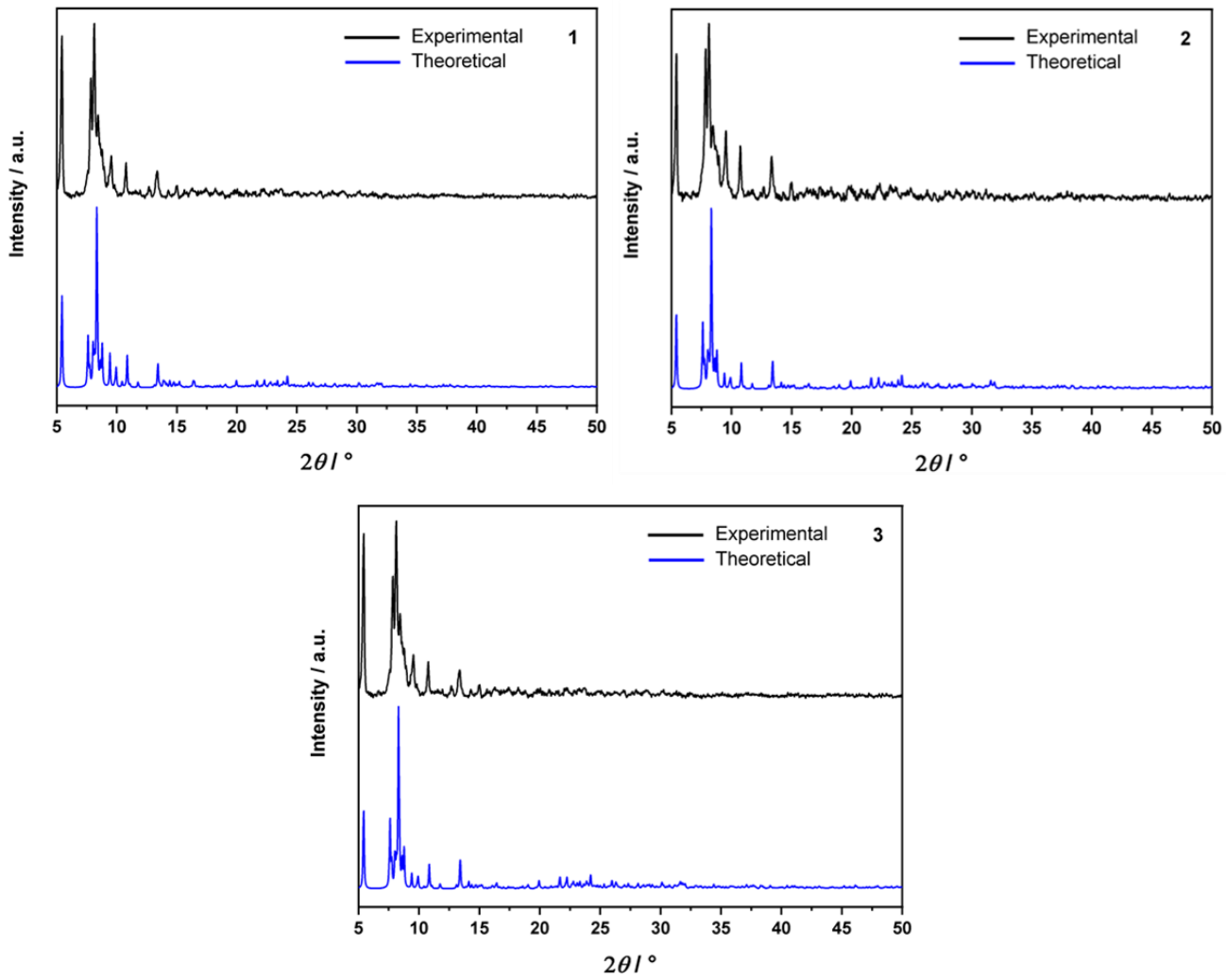

Fig. S5. Experimental powder X-ray diffraction (PXRD) spectra of **1**–**3** measured at RT (top) and, theoretical PXRD pattern calculated from single-crystal X-ray diffraction data (bottom). Homogeneity of the polycrystalline samples, used in the SQUID measurements, is evident by comparison of experimental *vs.* theoretical data.

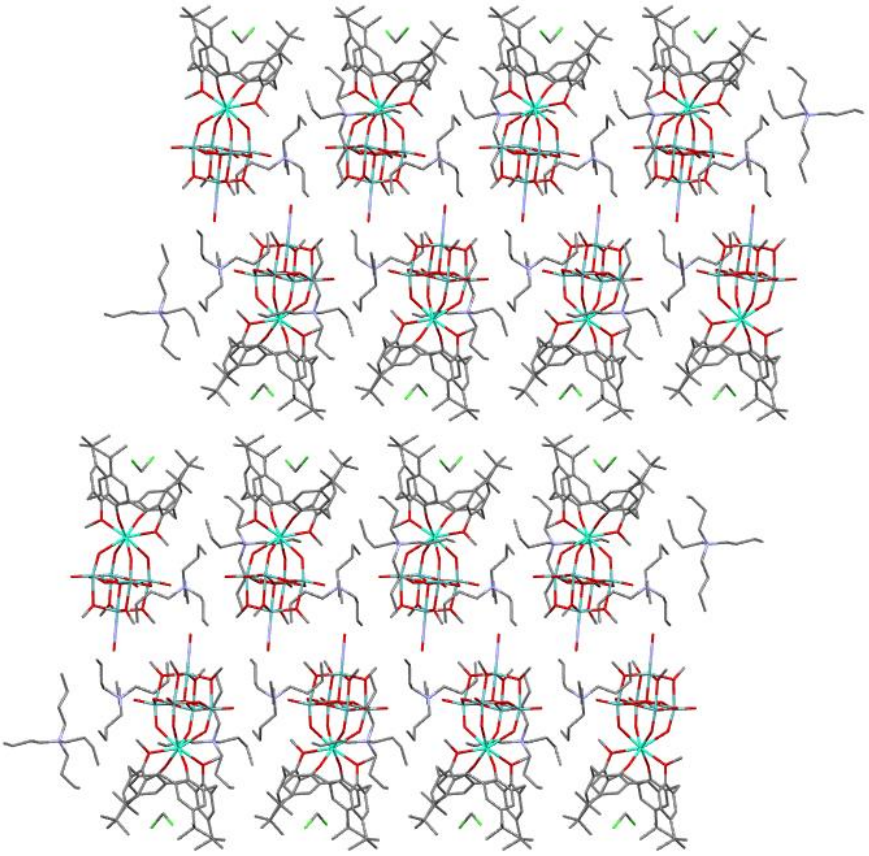

Fig. S6. Extended structure of **3** showing the packing into antiparallel bilayer arrays with interdigitated molecules. DCM molecules are encapsulated in the TBC[4] cavities, $(N(n\text{Bu})_4)^+$ counter cations crystallise in the interstitial space.

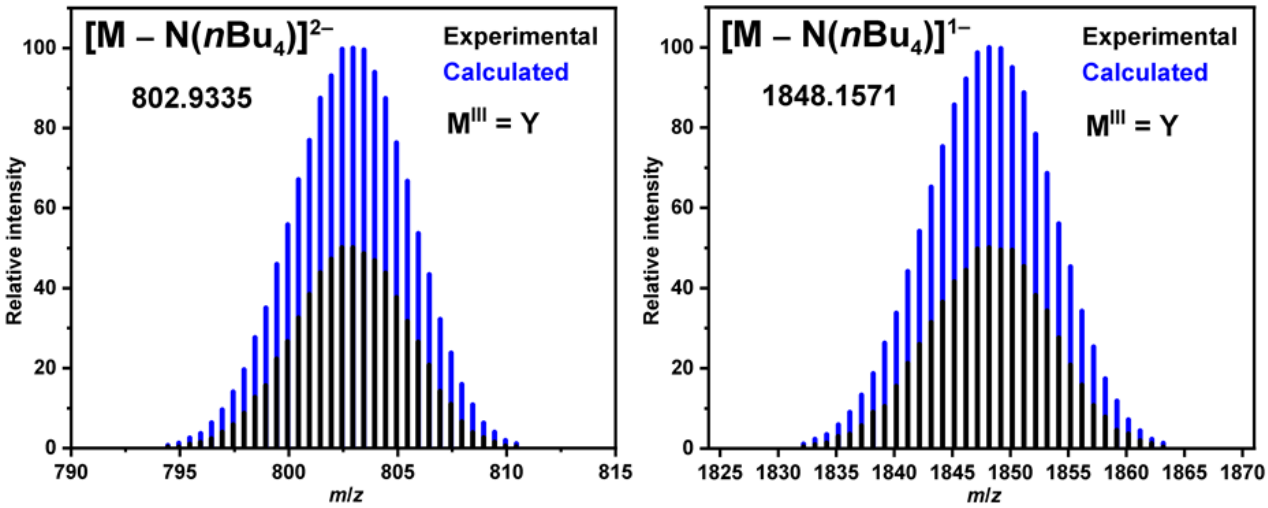

Fig. S7. ESI-HRMS spectra of $(N(n\text{Bu})_4)_2[Y^{III}L\{Mo_5O_{13}(OMe)_4(NO)\}]$ (**1**). (**Left**) *m*/*z*, found 802.9335 $[M - 2\ N(n\text{Bu})_4]^{2-}$ (34.3%), calculated for $[C_{50}H_{70}NO_{22}Mo_5Y]^{2-}$ 802.9385. (**Right**) *m*/*z*, found 1848.1571 $[M - N(n\text{Bu})_4]^{1-}$ (7.6%), calculated for $[C_{66}H_{106}N_2O_{22}Mo_5Y]^{1-}$ 1848.1614. M stands for $(N(n\text{Bu})_4)_2[Y^{III}L\{Mo_5O_{13}(OMe)_4(NO)\}]$. Experimental relative intensity values have been adjusted to 50% for the purpose of comparison.

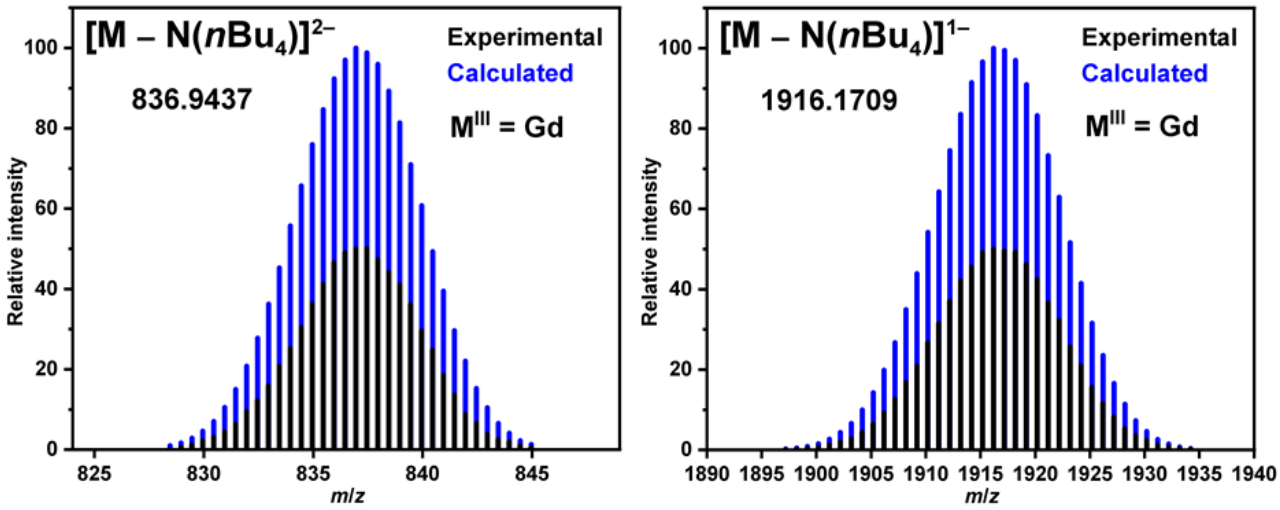

Fig. S8. ESI-HRMS spectra of $(N(n\text{Bu})_4)_2[Gd^{III}L\{Mo_5O_{13}(OMe)_4(NO)\}]$ (**2**). (**Left**) *m*/*z*, found 836.9437 [M – 2 $N(n\text{Bu})_4]^{2-}$ (32.9%), calculated for $[C_{50}H_{70}NO_{22}Mo_5Gd]^{2-}$ 836.9474. (**Right**) *m*/*z*, found 1916.1709 [M – $N(n\text{Bu})_4]^{1-}$ (100%), calculated for $[C_{66}H_{106}N_2O_{22}Mo_5Gd]^{1-}$ 1916.1796. M stands for $(N(n\text{Bu})_4)_2[Gd^{III}L\{Mo_5O_{13}(OMe)_4(NO)\}]$. Experimental relative intensity values have been adjusted to 50% for the purpose of comparison.

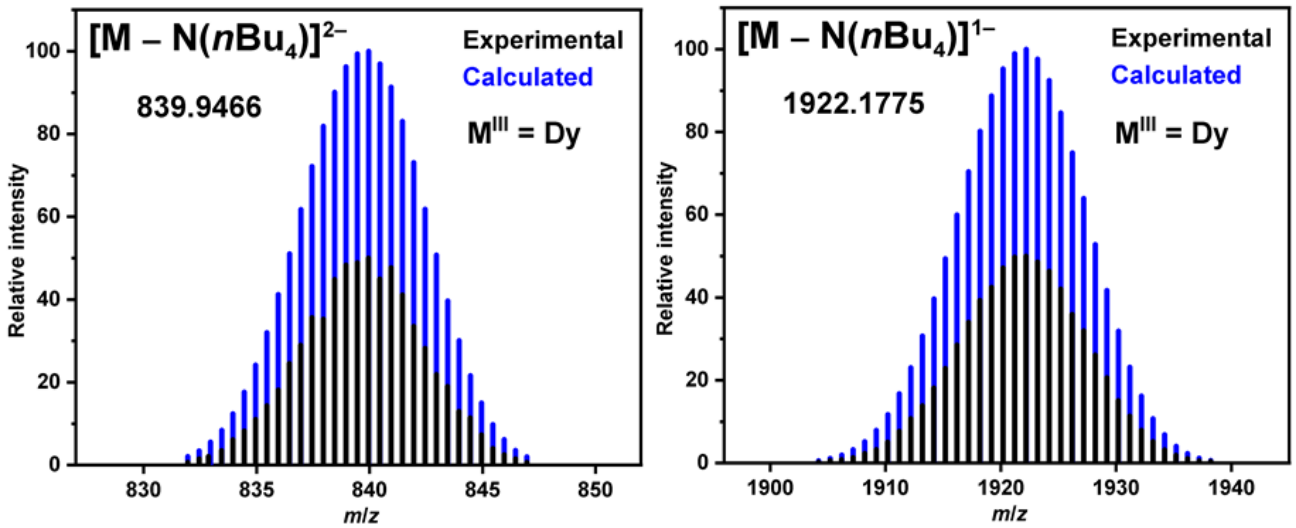

Fig. S9. ESI-HRMS spectra of $(N(n\text{Bu})_4)_2[Dy^{III}L\{Mo_5O_{13}(OMe)_4(NO)\}]$ (**3**). (**Left**) *m*/*z*, found 839.9466 [M – 2 $N(n\text{Bu})_4]^{2-}$ (12.1%), calculated for $[C_{50}H_{70}NO_{22}Mo_5Dy]^{2-}$ 839.9495. (**Right**) *m*/*z*, found 1922.1775 [M – $N(n\text{Bu})_4]^{1-}$ (100%), calculated for $[C_{66}H_{106}N_2O_{22}Mo_5Dy]^{1-}$ 1922.1836. M stands for $(N(n\text{Bu})_4)_2[Dy^{III}L\{Mo_5O_{13}(OMe)_4(NO)\}]$. Experimental relative intensity values have been adjusted to 50% for the purpose of comparison.

3 – Magnetic studies

We fitted the data of **2** and **3** using the computational framework CONDON.[3] For **2**, we used the isotropic spin-only option, while we employed the 'full' model option for **3**. The least-squares fits of both $\chi_m T$ *vs*. T curves (0.1 and 1.0 T) and the magnetisation curve at 2.0 K yield g_{eff} = 1.98±0.01 for the effective spin S_{eff} = 7/2 system of a Gd^{III} centre. The fit quality is very high, with a relative root mean squared error of SQ = 0.93 %. The effective g factor of **2** is slightly below the g factor of the free electron due to the mixing of excited terms into the ground term caused by the spin-orbit coupling.[4] Note the minor but noticeable deviation of the $\chi_m T$ values between fit and experimental data at 0.1 T below 10 K (Fig. S10, inset left), which is indicative of a small zero-field splitting. For the determination of the magnetic properties of **3**, the simple effective spin model is not sufficient. We, thus, use the 'full' model and treat the Slater-Condon parameters F^k (describing the electron-electron repulsion) and the one electron spin-orbit coupling parameter ζ_{4f} as constant. All 3003 microstates of the $4f^9$ valence electron configuration are considered in fitting the data in terms of the ligand field parameters B^k_q. For starting values, we use the REC model[5] that yields a set of parameters of an (almost) C_{2v} symmetric ligand field. Therefore, we assume a C_{2v} symmetric ligand field to reduce the number of fitting parameters. The respective least-squares fits are shown in Fig. S11 and S12 as solid lines, and the corresponding parameters are given in Table S1. The quality of the simultaneous fit of the $\chi_m T$ *vs*. T data at 0.1 and 1.0 T and the M_m *vs*. B data at 2.0 K is SQ = 0.78 %. The calculated energies and the wave functions of the ground term ($2J$+1 = 16 states) are shown in Table S2. The energy states are strongly mixed, although the respective main contribution of at least 57 % can be identified for each state. As a further feature, the ground doublet and first excited doublet are almost degenerate states. They are merely separated by about 0.2 cm^{-1}, which may be a reason for the need to apply the static bias field for better out-of-phase signals in the following ac measurements.

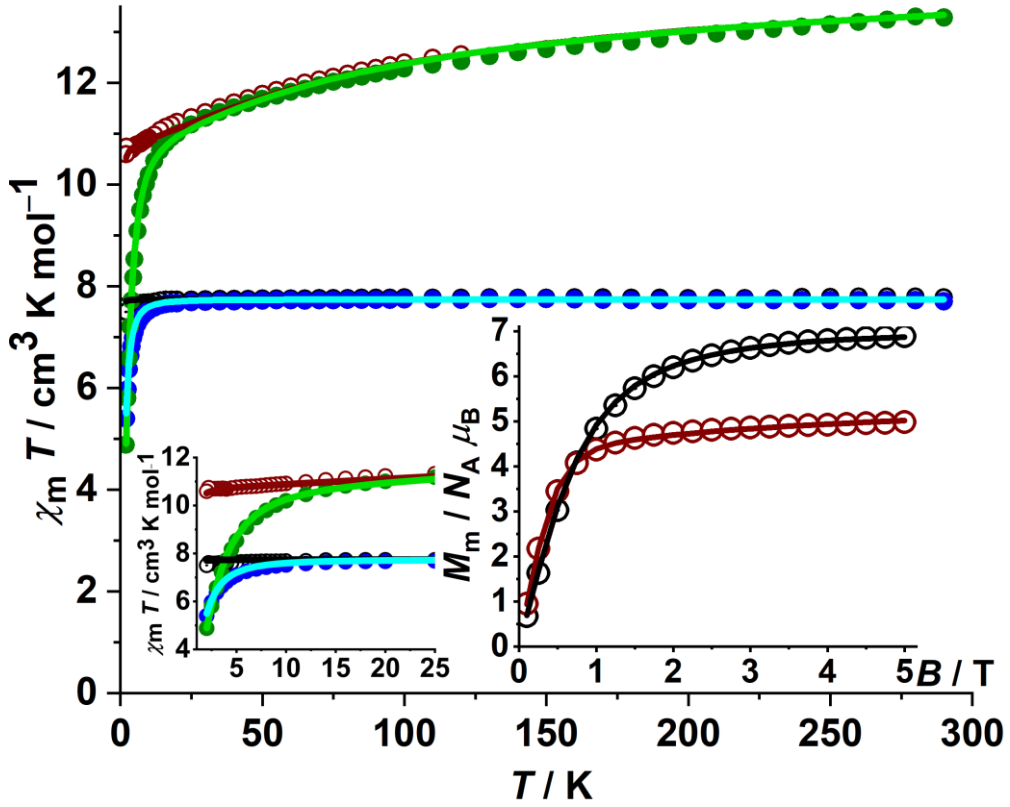

Fig. S10. Magnetic dc data: $\chi_m T$ *vs.* T at 0.1 (empty circles: **2** black and **3** brown colours) and 1T (filled circles: **2** blue and **3** green colours) and, M_m *vs.* B at 2.0 K (inset, right) for **2** (black empty circles) and **3** (brown empty circles); solid lines represent least-squares fit.

Table S1. Ligand field parameters of least-squares fits of the magnetic data of **3** in Wybourne notation. Slater-Condon parameters F^2 = 94500 cm^{-1}, F^4 = 66320 cm^{-1}, F^6 = 50707 cm^{-1}, and the one electron spin-orbit coupling constant ζ_{4f} = 1900 cm^{-1} were taken from literature. [6]

	B^k_0 / cm^{-1}	B^k_2 / cm^{-1}	B^k_4 / cm^{-1}	B^k_6 / cm^{-1}
k = 2	–176±5	–252±4		
k = 4	–2153±19	–1991±24	+273±85	
k = 6	–1172±9	+1364±7	+1185±33	+88±61

Measurements of **2** and **3** in dynamic (ac) magnetic fields revealed significant out-of-phase signals for **3**, particularly at a static magnetic bias field of 300 Oe. We analyse the data in terms of a generalised Debye expression[7] by simultaneously fitting of χ_m' *vs.* f and χ_m'' *vs.* f (Fig. S12). The fits yield the solid lines shown in Fig. S11a and S12. The corresponding relaxation times τ with the distribution α = 0.071±0.035 are plotted against the inverse temperature T shown in Fig. S11b. The value of α = 0.408±0.123 suggests the presence of a few relaxation pathways. By considering a direct and a Raman relaxation process, we find the best fit to the τ *vs.* $1/T$ data, *i.e.* using the equation $\tau^{-1} = A_{nK}T + CT^n$. The fit yields the parameter A_{nK} = (0.81±0.08) s^{-1} K^{-1} for the direct relaxation process, as well as C = (2.39±0.09)×10^{-4} s^{-1} K^{-n} and the exponent n = 7.1±0.1 for the Raman process. This is close to n = 7 indicating spin-two-phonon interaction with phonon energies larger than the energy between ground and excited state.[8] . In comparison with our previous report[1] the substitution of two

acac ligands by the {Mo_5} unit has a significant improvement of the slow relaxation behaviour. However, the found process parameters and, in particular, the temperature range of out-of-phase signal detection are quite common.

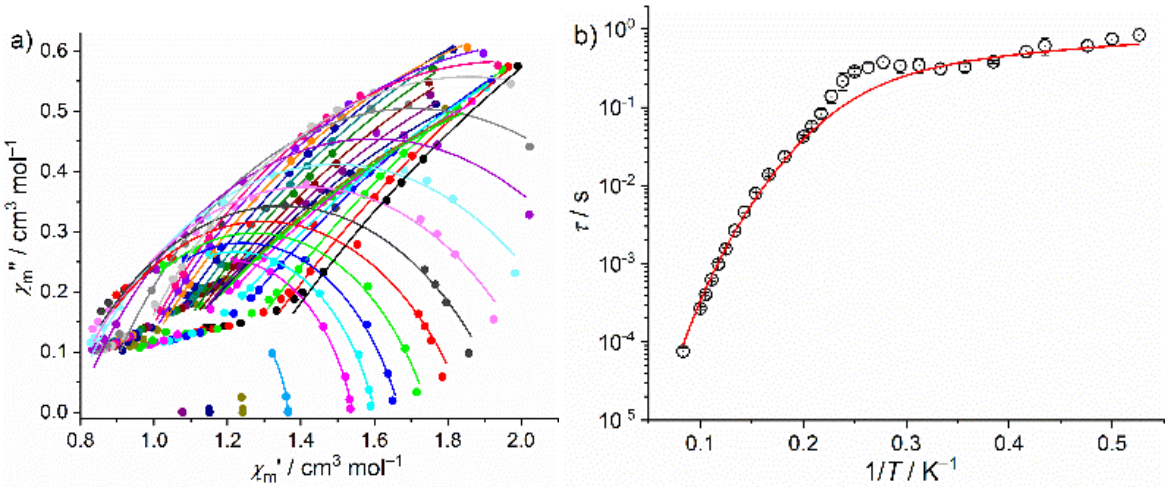

Fig. S11. (a) Magnetic ac data for **3**: Cole-Cole plot in the range 1.9–18.0 K at a static bias field of 300 Oe (filled circles: data, lines: fits to a generalised Debye expression, colour code: see Fig. S12b). **(b)** Plot of τ vs. T^{-1} (at 1.9 K $\leq T \leq$ 12.0 K) for **3**; the solid red line shows a combined fit considering a direct and a Raman slow relaxation process.

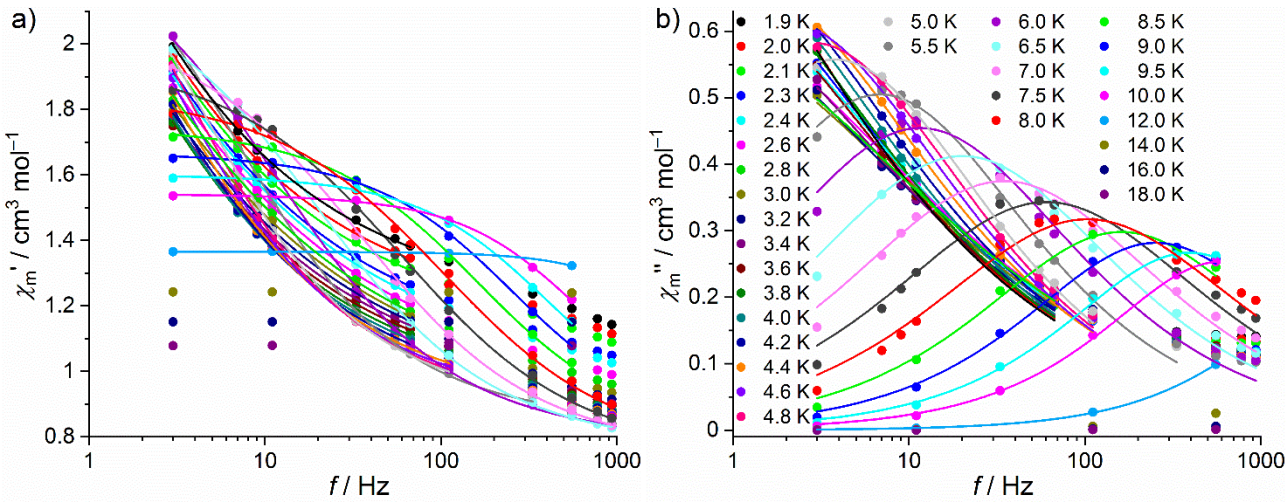

Figure S12. Magnetic ac data of **3** in the range 1.9–18.0 K at 300 Oe magnetic static bias field: (a) in-phase molar magnetic susceptibility χ_m' *vs.* applied frequency f, (b) out-of-phase molar magnetic susceptibility χ_m'' vs. f (filled circles: data, lines: fits to a generalised Debye expression.

Table S2. Energy levels relative to the ground state (at 0 cm^{-1}) and corresponding wave functions of the ground term of **3**. The $2J+1 = 16$ states are arranged in 8 doublets due to Dy^{III} being a Kramers ion; the kets $|m_J>$ indicate m_J according to Hellwege.

E / cm^{-1}	wave functions (upper signs for one energy state of the doublet, lower signs for the other; only listing contributions exceeding 1 %)
0	±0.60 |9/2> ± 0.18 |13/2> ∓ 0.14 |11/2> ∓ 0.04 |15/2> ± 0.02 |5/2> ∓ 0.01 |7/2>
0.15	±0.57 |11/2> ± 0.18 |15/2> ∓ 0.15 |9/2> ∓ 0.04 |13/2> ± 0.04 |7/2> ± 0.01 |3/2>
166	±0.85 |7/2> ± 0.08 |15/2> ± 0.03 |3/2> ± 0.02 |11/2> ∓ 0.02 |1/2>
290	±0.75 |5/2> ∓ 0.16 |3/2> ± 0.05 |9/2> ∓ 0.02 |7/2> ± 0.02 |1/2> ± 0.01 |13/2>
586	±0.75 |3/2> ∓ 0.11 |5/2> ∓ 0.06 |13/2> ∓ 0.03 |9/2> ∓ 0.02 |1/2> ± 0.02 |7/2>
651	±0.93 |1/2> ± 0.03 |5/2> ∓ 0.02 |7/2> ± 0.01 |13/2>
685	±0.71 |13/2> ± 0.16 |9/2> ± 0.09 |5/2> ∓ 0.04 |3/2>
940	±0.67 |15/2> ± 0.28 |11/2> ± 0.04 |7/2> ± 0.01 |3/2>

4 – Crystallographic analysis details

Single crystal diffraction data for **1**−**3** were collected on a STOE STADIVARI (**1**) and on a Rigaku SuperNova (**2** and **3**) diffractometers with MoKα radiation (λ = 0.71073 Å) at 100 K. The crystals were mounted on a Hampton cryoloop with Paratone-N oil to prevent water loss. Absorption corrections was applied numerically based on multifaceted crystal model using either STOE X-Red32 software[9] with the following scaling of reflection intensities performed within STOE LANA[10] for **1** or with a CrysAlis software for **2** and **3**.[11] The SHELXTL software package[12] was applied to solve and refine the structures. The structures were solved by direct methods and refined by full-matrix least-squares method against $|F|^2$ with anisotropic thermal parameters for all non-hydrogen atoms (Ln, Mo, O, Cl, N and C). ISOR restrictions had to be applied for some C atoms of the tert-butyl groups of the TBC[4]. Hydrogen atoms were placed in geometrically calculated positions.

Additional crystallographic data are summarised in Table S3. Further details on the crystal structures investigation can be obtained, free of charge, on application to CCDC, 12 Union Road, Cambridge CB2 1EZ, UK: http://www.ccdc.cam.ac.uk/, e-mail: data_request@ccdc.cam.ac.uk, or fax: +441223 336033 upon quoting 2143146 (**1**), 2143147 (**2**) and 2143149 (**3**) numbers. Some selected bond lengths in complexes **1**–**3** are shown in Table S4.

Table S3. Crystal data and structure refinement for **1**–**3**.

Sample	**1**	**2**	**3**
Empirical formula	$C_{84.5}H_{147}O_{22}N_3Cl_5Mo_5Y$	$C_{83}H_{144}O_{22}N_3Cl_2Mo_5Gd$	$C_{83}H_{144}O_{22}N_3Cl_2Mo_5Dy$
Formula weight / g mol^{-1}	2302.90	2243.85	2249.10
Crystal system	Triclinic	Monoclinic	Monoclinic
Space group	*P*−1	*C*2/*c*	*C*2/*c*
a / Å	13.449(3)	67.2987(15)	67.0340(6)
b / Å	14.984(3)	12.5266(2)	12.5392(1)
c / Å	27.024(5)	23.4455(4)	23.4462(2)
α	102.94(3)°	90°	90°
b	93.170(2)°	103.345(2)°	103.174(1)°
γ	101.77(3)°	90°	90°
Volume / Å^3	5036(2)	19231.4(6)	19189.1(3)
Z	2	8	8
D_{calc} / g cm^{-3}	1.519	1.550	1.557
Absorption coefficient / mm^{-1}	1.371	1.434	1.525
F(000)	2370	9176	9192
Crystal size / mm^3	0.05 × 0.11 × 0.22	0.03 × 0.055 × 0.20	0.07 × 0.11 × 0.42
Theta range for data collection	2.28° – 25.02°	3.18° – 25.02°	3.21° – 25.02°
Completeness to Q_{max}	99.6 %	99.8 %	99.8 %
Index ranges	–16 < *h* < 9, –17 < *k* < 17, –32 < *l* < 32	–78 < *h* < 80, –14 < *k* < 14, –27 < *l* < 27	–79 < *h* < 79, –14 < *k* < 14, –27 < *l* < 27
Reflections collected	92044	84378	172457

Independent reflections	17716	16931	16905
R_{int}	0.0927	0.0770	0.0764
Observed ($I > 2\sigma(I)$)	11169	12688	14508
Absorption correction	Gaussian integration	Analytical	Analytical
T_{min} / T_{max}	0.7589 / 0.9432	0.8810 / 0.9900	0.4290 / 0.9210
Data / restraints / parameters	17716 / 12 / 1099	16931 / 12 / 1045	16905 / 6 / 1045
Goodness-of-fit on F^2	1.043	1.052	1.084
R_1, wR_2 ($I > 2\sigma(I)$)	R_1 = 0.0794, wR_2 = 0.2056	R_1 = 0.0430, wR_2 = 0.0894	R_1 = 0.0388, wR_2 = 0.0835
R_1, wR_2 (all data)	R_1 = 0.1266, wR_2 = 0.2388	R_1 = 0.0697, wR_2 = 0.1039	R_1 = 0.0499, wR_2 = 0.0902
Largest diff. peak and hole / e Å^{-3}	17716 / –1.688	1.533 / –1.500	1.720 / –1.576

Table S4. Selected bond lengths (Å) in complexes **1**–**3**.

Bond type	**1**	**2**	**3**
Ln–O_L	2.117(6)-2.140(6)	2.141(3)-2.155(3)	2.117(3)-2.136(3)
Ln–$O_{L(OMe)}$	2.496(6)-2.574(6)	2.551(3)-2.573(3)	2.534(3)-2.561(3)
Ln–$O_{[Mo5O13(OMe)4(NO)]}$	2.428(6)-2.479(6)	2.463(3)-2.483(3)	2.432(3)-2.508(3)
Mo_1–O	1.990(6)-2.121(6)	1.981(4)-2.119(3)	1.992(3)-2.117(3)
$Mo_{2\text{-}5}$–O	1.670(6)-2.326(6)	1.692(3)-2.357(3)	1.700(3)-2.357(3)

References

[1] Y. Jiao, Sidra Sarwar, S. Sanz, J. van Leusen, N. V. Izarova, C. L. Campbell, E. K. Brechin, S. J. Dalgarno and P. Kögerler, *Dalton Trans.*, 2021, **50**, 9648–9654.

[2] A. Proust, P. Gouzerh and Francis Robert, *Inorg. Chem.*, 1993, **32**, 5291–5298.

[3] M. Speldrich, J. van Leusen and P. Kögerler, *J. Comput. Chem.*, 2018, **39**, 2133–2145.

[4] J. Sytsma, K. M. Murdoch, N. M. Edelstein, L. A. Boatner and M. M. Abraham, *Phys. Rev.* B, 1995, **52**, 12668–12676.

[5] a) J. J. Baldovi, J. J. Borras-Almenar, J. M. Clemente-Juan, E. Coronado and A. Gaita-Arino, *Dalton Trans.* 2012, **41**, 13705–13710; b) J. J. Baldovi, A. Gaita-Arino and E. Coronado, *Dalton Trans.* 2015, **44**, 12535–12538.

[6] E. U. Condon and G. H. Shortley, *The Theory of Atomic Spectra*, Cambridge University Press, Cambridge, 1970.

[7] K. S. Cole and R. H. Cole, *J. Chem. Phys.*, 1941, **9**, 341–351.

[8] a) K. N. Shrivastava, *Phys. Status Solidi B* 1983, **117**, 437–458. b) A. Singh and K. N. Shrivastava, *Phys. Status Solidi B*, 1979, **95**, 273–277.

[9] STOE X-Red32, absorption correction by Gaussian integration, analogous to P. Coppens, The Evaluation of Absorption and Extinction in Single-Crystal Structure Analysis. Crystallographic Computing (Ed.: F. R. Ahmed), Munksgaard, Copenhagen, 1970, 255–270.

[10] J. Koziskova, F. Hahn, J. Richter and J. Kožíšek, *Acta Chim. Slov.*, 2016, **9**, 136–140.

[11] CrysAlisPro, Agilent Technologies, 1.171.36.28 (release 01-02-2013 CrysAlis171 .NET).

[12] G. M. Sheldrick, *Acta Cryst.*, 2015, **C71**, 3–8.